International Journal of Computer Vision 25(2), 95–107 (1997)

Affine Morphological Multiscale Analysis of Corners and Multiple Junctions

LUIS ALVAREZ AND FREYA MORALES*
Departamento de Informatica y Sistemas, Universidad de Las Palmas de Gran Canaria, Campus de Tafira, 35017 Las Palmas, Spain
luis@amihp710.dis.ulpgc.es
freya@amihp710.dis.ulpgc.es

Received October 4, 1994; Accepted July 12, 1995

Abstract. In this paper we study the application of the Affine Morphological Scale Space (AMSS) to the analysis of singularities (corners or multiple junctions) of the shapes present in a 2-D image. We introduce a new family of travelling wave solutions of AMSS which determines the evolution of the initial shapes given by conics. We characterize the evolution of corners accross the scales according to their angle. We develop a numerical algorithm to compute AMSS accross the scales and we present some experimental results about corners and multiple junction detection.

Keywords: scale space, mathematical morphology, invariant theory, corner detector, multiple junctions

1. Introduction

A simple model to discuss image processing is to define an "image" as a "brightness" function $u_0(x, y)$ at each point (x, y) of a domain of the plane. This domain, which may be the plane itself, is a model of the retina or of any other photosensitive surface. In what follows, we shall take the plane for simplicity.

One of the main concepts of vision theory and image analysis is *multiscale analysis* (or "*scale space*"). Multiscale analysis associates, with $u(0) = u_0$, a sequence of simplified (smoothed) images $u(t, x, y)$ which depend upon an abstract parameter $t > 0$, the *scale*. The image $u(t, x, y)$ is called *analysis of the image* u_0 *at scale* t. The formalization of *scale space* has received a lot of attention in the last ten years; more than a dozen of theories for image, shape or "texture" multiscale analysis have been proposed and recent mathematical work has permitted a formalization of the whole field. See (Alvarez et al., 1992; Asada and Brady, 1986; Gage and Hamilton, 1986; Julesz, 1981; Koenderink, 1984; Mackworth and Mokhtarian, 1986; Marr, 1982; Matheron, 1975; Sapiro and Tannenbaum, 1994; Serra, 1982; Witkin, 1983).

The datum of $u_0(x, y)$ is not absolute in perception theory, but can be considered as the element of an equivalence class. If R is an isometry of the plane, $u_0(R(x, y))$ is an equivalent datum and the visual analysis must be the same. In the same way, $u_0(x, y)$ and $u_0(A(x, y))$, where A is any affine map of the plane, can be assumed equivalent from a perceptual point of view. Last but not least, the observation of $u_0(x, y)$ does not generally give any reliable information about the number of photons sent by any visible place to the optical sensor. Therefore, the equivalence class in consideration will be $g(u_0(A(x, y)))$, where g stands for any (unknown) contrast function depending on the sensor. This last assumption, that only isophotes matter, is associated with the "mathematical morphology" school. So we shall call it the "morphological" assumption.

We must keep in mind that the multiscale analysis acts on equivalence classes of images whose form is $g(u_0(Ax))$, where g is any nondecreasing continuous

*This research was partially supported by the C.I.C.Y.T., Spain project TIC 92-1282.

function and A any affine map, and that the multiscale analysis should not depends on the choice of g or A. These considerations lead us to focus on the only multiscale analysis which satisfies these invariance requirements: the Affine Morphological Scale Space (AMSS). This multiscale analysis can be defined by a simple Partial Differential Equation,

$$u_t = t^{\frac{1}{3}}\left(u_y^2\, u_{xx} - 2u_x u_y\, u_{xy} + u_x^2\, u_{yy}\right)^{\frac{1}{3}} \qquad (1)$$

where $u(t, x, y)$ denotes the image analyzed at scale t and the point (x, y). This Multiscale Analysis has been discovered independently by Sapiro and Tannenbaum (1993, 1994) and Alvarez et al. (1992, 1993). Cohignac et al. (1993) have proposed different schemes to discretize the above equation.

The main goal of this paper is to analyze how the singularities in the image, as corner and multiple junctions, evolve across the scales and to show how this information can be used to characterize the shape of the singularities following their evolution across the different scales. We consider that a Shape X in the image is given by the boundary of a level set of $u_0(x, y)$, $X = \partial\{(x, y) : u_0(x, y) > C\}$. For instance, in this paper we consider that a canonical representative of a corner of angle $\frac{\pi}{2}$ is any function $u_0(x, y)$ such that there exists a constant C verifying $X = \partial\{(x, y) : u_0(x, y) > C\} = \{(x, y) : y = |x|\}$.

We follow the evolution of a Shape across the scales analyzing the evolution of the level set

$$X(t) = \partial\{(x, y) : u(t, x, y) > C\}$$

where $u(t, x, y)$ corresponds to the solution of Eq. (1). For instance, if $X(0)$ is a corner of angle $\frac{\pi}{2}$ we will show that its evolution $X(t)$ across the scales using the AMSS model is given by the branch of hyperbole (see Fig. 1). Moreover, following the evolution of the curvature extrema points, we will show that the corner itself evolves following the bisector line and at the scale t the displacement with respect to the initial position is equal to t.

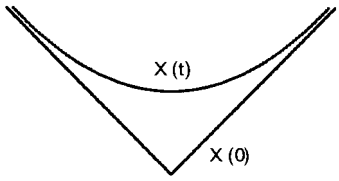

Figure 1. Representation of a corner, $X(0)$, of angle $\frac{\pi}{2}$ and its evolution $X(t)$.

In the framework of the AMSS scale space this result can be easily extended to any corner of angle α with $0 < \alpha < \pi$. Indeed, a corner of angle α can be interpreted as an affine transformation of a corner of angle $\frac{\pi}{2}$ and therefore, using the affine invariance of AMSS, we can easily show, as we will see, that a corner of angle α evolves following the bisector line and at the scale t the displacement with respect to the initial position is equal to $\tan(\frac{\alpha}{2})^{-\frac{1}{2}}t$. With this last formula we characterize the angle of the corner following the displacement velocity across the scales.

Usually, as it was noticed by Deriche and Giraudon (1993), the analysis of multiple junctions is much more complex than the analysis of corners. A very important advantage of the AMSS model is that, as we will show, in this framework, a multiple junction can be interpreted as a simple collection of corners, and the evolution across the scales of a multiple junction corresponds to the evolution of several corners which evolve in an independent way.

The remainder of this article is organized as follows: Section 2 presents an overview of some previous works about corner and junction detections. We will point out the main difference between our approach using the AMSS scale space and another scale space framework such as the linear gaussian scale space. In Section 3 we compute explicitly the analytical expression of some travelling waves solutions of AMSS. We will use these solutions to characterize the evolutions of Shapes given by conics. In Section 4, we characterize the evolution of corners and multiple junctions across the scales using AMSS. In Section 5 we present an algorithm to compute, numerically, AMSS. In Section 6 we present some numerical results of corner and multiple junction analysis and detection. Finally in Section 7, we present the main conclusions of this paper.

2. Connection with Some Related Works

The differential operator of the right part of Eq. (1) is not new in the framework of corner analysis. For instance, Kitchen and Rosenfeld (1982) proposed a measure of cornerness based on the local maxima of the operator

$$\frac{u_y^2\, u_{xx} - 2u_x u_y\, u_{xy} + u_x^2\, u_{yy}}{u_x^2 + u_y^2}$$

which corresponds to the second directional derivative in the direction orthogonal to the gradient. The curvature in a point (x, y) of a level line $X(t)$ is defined by the operator:

$$\text{curv}(u) = \frac{u_y^2\, u_{xx} - 2u_x u_y\, u_{xy} + u_x^2\, u_{yy}}{\left(u_x^2 + u_y^2\right)^{\frac{3}{2}}} \qquad (2)$$

Beaudet (1978) proposed a rotationally invariant differential operator called DET:

$$\text{DET} = u_{xx}\, u_{yy} - u_{xy}^2 \qquad (3)$$

The corner detection is based on the thresholding of the absolute value of the extrema of this operator.

Different authors have proposed models based on the gaussian linear scale space analysis to improve this kind of measure. Lindeberg (1993) use the above measure, but at different scales, to extract information about the corners present in the image.

Deriche and Giraudon (1993) have developed a complete and interesting analytical study of corner models using the linear gaussian scale space. They define an ideal corner of angle α as a grey level image $u_0(x, y)$ which corresponds to a characteristic function. $u_0(x, y) = U(mx - y)U(y)$ where $m = \tan(\alpha)$ and $U(x) = 1$ if $x > 0$ and $U(x) = 0$ otherwise. They analyze the evolution across the scales (in the linear gaussian scale space) of an ideal corner using the local maximum of different measures of cornerness as the Beaudet measure (DET) or using the gaussian curvature proposed by Dreschler and Nagel (1982). They show that the local maximum moves in the scale space along the bisector line that passes through the exact position of the corner point. They also show that the displacement of the local maximum with respect to the initial location of the corner depend on the angle α and the choice of measure of cornerness. Basing on this analytical study, they propose an algorithm to extract the corner location following their evolution across the scales. Recently Deriche (1994) has stayed a numerical procedure to obtain the exact angle of the corner that corresponds to a displacement velocity of the corner along the bisector line in the linear gaussian scale space using different cornerness measures. In Fig. 2 we compare the displacement velocity of a corner following its angle using the results obtained by Deriche for the gaussian scale space and the displacement velocity that we obtain in this paper for the AMSS scale space. As we will show we can stay a very simple relation between the angle α of the corner and the displacement velocity of the corner across the scales (velocity $(\alpha) = (\tan(\frac{\alpha}{2})^{-\frac{1}{2}})$.

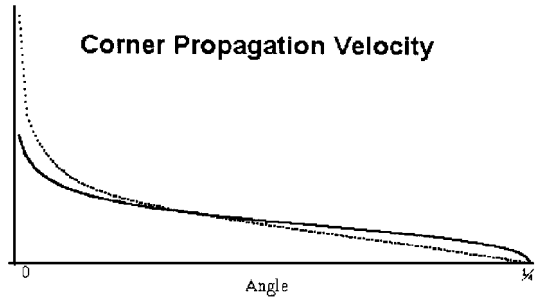

Figure 2. Displacement velocity of a corner following the extremum curvature points across the scales. In the x-axe we represent the angle of the corner, and in the y-axe the displacement velocity. The dashed line corresponds to the linear gaussian scale-space, and the continuous line corresponds to the AMSS scale space.

In a more recently paper, Rohr (1994) analyzes the displacement of the location of the corners using an analytical model of the corners which introduces a smoothing procedure given by a gaussian function. However, such analytical model of the corner does not correspond to the model of Deriche and Giraudon.

The analysis of corners that we present in this paper is close to the analysis of Deriche and Giraudon in the sense that we introduce a model of corner and we study the evolution of corners across the scales in order to extract information about the corners present in the image. However, there are some fundamental differences between their approach and our approach due basically to the invariance properties of the AMSS scale space.

The first fundamental difference is about the model of corner. We use a "level set" definition. It means that we define an ideal corner, X, as the boundary of a level set of a grey-level image $X = \partial\{(x, y) : u_0(x, y) > C\}$. In this framework the model of Deriche and Giraudon corresponds to a particular choice of image $u_0(x, y)$ given by a characteristic function where the corner corresponds to the boundary of the level set $C = 0$. The choice of characteristic functions is rigid because it is not allowed grey level fluctuations in the description of the corner. However, using our "level set" definition we can allow this kind of grey level fluctuations. The only important fact is that, for some grey level C, the boundary of the level set is an ideal corner. For instance, in the mathematical analysis of corners using the AMSS scale space that we present in this

paper we use, as model of corner, the following smooth function:

$$u_0(x,y) = \begin{cases} \left(\left(\frac{y}{\lambda}\right)^2 - (\lambda x)^2\right)^2 & \text{if } y \geq \lambda^2 |x| \\ 0 & \text{otherwise} \end{cases}$$

where the corner corresponds to the boundary of the level set $C = 0$.

This "level set" model of corners is closely related to the morphological invariance of the AMSS scale space. Indeed, due to the morphological invariance, the evolution across the scales of a shape X does not depend on the choice of function $u_0(x, y)$ where this shape is included. Of course, this is not true in the case of the linear gaussian scale space where this "level set" definition has not sense.

On the other hand, the morphological invariance imposes some restrictions in the choice of the measure of the cornerness to follow the point (t, x, y) in the shape $X(t)$ which represents the evolution of the corner itself across the scales. Indeed, the measure of cornerness that we use must be invariant if we change $u(t, x, y)$ by $g(u(t, x, y))$ where $g(\cdot)$ is any increasing continuous function. It is not difficult to show that the curvature of the level lines, given by Eq. (2) satisfies this invariance, but the Hessian (DET) or the Gaussian Curvature does not satisfy this invariance.

The concept of corner is affine invariant in the sense that for any angle α, with $0 < \alpha < \pi$ there exists an affine transformation which transforms this corner into a canonical corner, for instance, of angle $\frac{\pi}{2}$. Therefore, if we characterize the evolution of a corner of angle $\frac{\pi}{2}$ across the scales using AMSS, then, due to the affine invariance, we can characterize easily the evolution of a corner of any angle α. This last property unifies the analysis of corners in the AMSS framework. We notice that, in the case of the linear gaussian scale space, a different study must be done for each different angle of corner.

Another important difference of the AMSS approach with respect to the linear gaussian scale space approach is the analysis of the multiple junctions. In the linear case, the evolution across the scales of the image produces a diffusion which blends the information of different level sets and the analysis of a multiple junction becomes very complex as (Deriche and Giraudon, 1993) showed in the case of trihedral vertex. However, as we will show in Section 4, in the framework of AMSS, the analysis of a multiple junction is reduced to the analysis of some corners which evolves in an independent way.

Merriman et al. (1992) address the problem of multiple junctions evolution in a different context. They consider a multiple junction as a partition of $\Re^2$ into regions R_i which correspond to the different components of the multiple junction. They compute the motion of the multiple junction using the following algorithm:

1. For each region a R_i, we compute the characteristic function χ_i of the region R_i.
2. We diffuse each χ_i independently for some time T_{chop} using a P.D.E. as for instance the heat equation.
3. We set $\chi_i = \{x : \chi_i(x) > \chi_j(x), \text{ for any } j\}$.
4. Go to (2).

We notice that the point of view of Merriman, Bence and Osher is completely different to the ideas presented in this paper.

3. Travelling Waves Solutions of AMSS

Due to the invariance properties of the multiscale analysis AMSS, the analysis of a Shape is completely independent of the position of the Shape and the relative contrast with other shapes which are present in the image. It means, in particular, that the smoothness of the initial datum $u_0(x, y)$ is not a relevant point in our analysis. For simplicity, we are going to consider that $u_0(x, y)$ is a smooth function $u_0 \in C^2(\Re^2, \Re)$.

Theorem 1. *Let $\lambda > 0$ be a positive number and $h \in C^2(\Re : \Re)$. Then the following functions are solutions of AMSS*:

(i) $u^e_\lambda(t, x, y) = h(((\frac{y}{\lambda})^2 + (\lambda x)^2)^{\frac{2}{3}} + t^{\frac{4}{3}})$

(ii) $u^p_\lambda(t, x, y) = h(\frac{y}{\lambda} - (\lambda x)^2 - \frac{3}{32^{\frac{1}{3}}} t^{\frac{4}{3}})$

(iii) *If $h'(0) = h''(0) = 0$*

$$u^h_\lambda(t, x, y) = \begin{cases} h\left(\left(\left(\frac{y}{\lambda}\right)^2 - (\lambda x)^2\right)^{\frac{2}{3}} - t^{\frac{4}{3}}\right) & \text{if } \left(\frac{y}{\lambda}\right)^2 - (\lambda x)^2 - t^2 \geq 0 \\ h(0) & \text{if } \left|\left(\frac{y}{\lambda}\right)^2 - (\lambda x)^2\right| < t^2 \\ h\left(-\left(\left(\frac{y}{\lambda}\right)^2 - (\lambda x)^2\right)^{\frac{2}{3}} + t^{\frac{4}{3}}\right) & \text{if } \left(\frac{y}{\lambda}\right)^2 - (\lambda x)^2 + t^2 \leq 0 \end{cases}$$

Proof: First, we notice that due to the affine invariance property of AMSS we can fix $\lambda = 1$. Next we look for the solution of AMSS which can be written explicitly as

$$u(t, x, y) = H(t, g(x, y))$$

if we take $z = g(x, y)$ we obtain:

$$\begin{aligned} u_t &= H_t \\ u_x &= g_x H_z \\ u_y &= g_y H_z \\ u_{xx} &= g_{xx} H_z + g_x^2 H_{zz} \\ u_{yy} &= g_{yy} H_z + g_y^2 H_{zz} \\ u_{xy} &= g_{xy} H_z + g_x g_y H_{zz} \end{aligned}$$

and we obtain that AMSS is equivalent to

$$H_t = t^{\frac{1}{3}} \left(g_y^2 g_{xx} - 2 g_x g_y g_{xy} + g_x^2 g_{yy}\right)^{\frac{1}{3}} H_z \qquad (4)$$

To simplify the analysis, now we look for the functions $g(x, y)$ such that:

$$\left(g_y^2 g_{xx} - 2 g_x g_y g_{xy} + g_x^2 g_{yy}\right) = a g(x, y) + b$$

where a, b are constants. Sapiro and Tannenbaum (1994) showed that the only functions that verify the above relations are the conics.

We have that if $g(x, y) = x^2 + y^2$ then

$$\left(g_y^2 g_{xx} - 2 g_x g_y g_{xy} + g_x^2 g_{yy}\right) = 8 g(x, y)$$

Therefore, in this case, Eq. (4) is equivalent to:

$$H_t = 2 t^{\frac{1}{3}} z^{\frac{1}{3}} H_z$$

Since $z \geq 0$, we can take $H(t, z) = G(t^{\frac{4}{3}}, z^{\frac{2}{3}})$ and we obtain that $G(\cdot, \cdot)$ satisfies the well known first order linear equation $G_t = G_z$. The solution of this equation is given by the travelling wave:

$$G(t, z) = h(t + z)$$

where $h(\cdot)$ represents the initial datum. Therefore, (i) follows taking $u_\lambda^e(t, x, y) = H(t, (\frac{y}{\lambda})^2 + (\lambda x)^2))$.

In order to proof (ii) we notice that if we take $g(x, y) = y - x^2$ then

$$\left(g_y^2 g_{xx} - 2 g_x g_y g_{xy} + g_x^2 g_{yy}\right) = -2$$

Therefore, in this case Eq. (4) is equivalent to:

$$H_t = -t^{\frac{1}{3}} 2^{\frac{1}{3}} H_z$$

We can take $H(t, z) = G(t^{\frac{4}{3}}, z)$ and we obtain that $G(\cdot, \cdot)$ satisfies $G_t = -\frac{3}{32^{\frac{1}{3}}} G_z$. The solution of this equation is given by the travelling wave: $G(t, z) = h(z - \frac{3}{32^{\frac{1}{3}}} t)$. Therefore (ii) follows taking $u_\lambda^p(t, x, y) = H(t, \frac{y}{\lambda} - (\lambda x)^2))$.

Finally, in order to proof (iii), first, we notice that if we take $g(x, y) = y^2 - x^2$ then

$$\left(g_y^2 g_{xx} - 2 g_x g_y g_{xy} + g_x^2 g_{yy}\right) = -8 g(x, y)$$

Therefore, in this case, Eq. (4) is equivalent to:

$$H_t = -2 t^{\frac{1}{3}} z^{\frac{1}{3}} H_z$$

In the region where $z \geq 0$ we can take $H(t, z) = G(t^{\frac{4}{3}}, z^{\frac{2}{3}})$ and we obtain that $G(\cdot, \cdot)$ satisfies $G_t = -G_z$. The solution of this equation is given by the travelling wave: $G(t, z) = h(z - t)$.

In the region where $z \leq 0$ we can take $H(t, z) = G(t^{\frac{4}{3}}, -z^{\frac{2}{3}})$ and we obtain that $G(\cdot, \cdot)$ satisfies $G_t = G_z$. Since $G(\cdot, \cdot)$ is given by travelling waves with opposite directions and $h'(0) = h''(0) = 0$, then a classical solution of the above equation is given by:

$$G(t, z) = \begin{cases} h(z - t) & \text{if } z - t \geq 0 \\ h(0) & \text{if } |z| < t \\ h(z + t) & \text{if } z + t \leq 0 \end{cases}$$

Therefore (iii) follows taking $u_\lambda^h(t, x, y) = H(t, (\frac{y}{\lambda})^2 - (\lambda x)^2))$. □

Notice that the level sets of the travelling wave solution of AMSS showed above correspond to conics. In the case (i) the level sets are ellipses, the evolution of a level set across the scales is given by the formula

$$\left(\left(\frac{y}{\lambda}\right)^2 + (\lambda x)^2\right)^{\frac{2}{3}} + t^{\frac{4}{3}} = C$$

In the case (ii) the level sets correspond to parabolas, the evolution of a level set across the scales is given by the formula

$$\frac{y}{\lambda} - (\lambda x)^2 - \frac{3}{32^{\frac{1}{3}}} t^{\frac{4}{3}} = C$$

In the case (iii) the level sets are hyperboles, the evolution of the boundary of the level set across the

scales is given by the formula

$$\begin{cases} \left(\frac{y}{\lambda}\right)^2 - (\lambda x)^2 - t^2 = C & \text{if } C > 0 \\ \left|\left(\frac{y}{\lambda}\right)^2 - (\lambda x)^2\right| = t^2 & \text{if } C = 0 \\ \left(\frac{y}{\lambda}\right)^2 - (\lambda x)^2 + t^2 = C & \text{if } C < 0 \end{cases}$$

4. Characterization of Corners and Multiple Junctions Evolution

In this section, we are going to characterize the evolution of a corner of any angle α. As we are going to show, the way in which the corner evolves across the scales characterizes and identifies the corner. Without any loss of generality we will assume that the corner is placed in the point $(0, 0)$ and that the bisector line is $x = 0$.

Theorem 2. *Let X be a shape given by a corner of angle α. Let $\lambda = (\tan(\frac{\alpha}{2}))^{-\frac{1}{2}}$. Then the evolution of the corner is given by the shapes*

$$X(t) = \left\{(x, y) : y = \lambda(t^2 + (\lambda x)^2)^{\frac{1}{2}}\right\} \qquad (5)$$

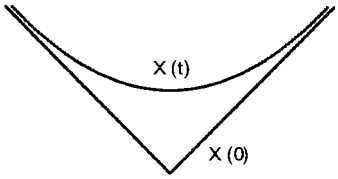

Moreover, the evolution of the corner itself, following the extrema points of the curvature across the scales is given by the formula $(0, \lambda t)$.

Proof: Using the same argument that we used in the proof of Theorem 1 (iii), we can show that for any $\lambda > 0$ the following function is a solution of AMSS

$$u_\lambda(t, x, y) = \begin{cases} \left(\left(\left(\frac{y}{\lambda}\right)^2 - (\lambda x)^2\right)^{\frac{2}{3}} - t^{\frac{4}{3}}\right)^3 & \text{if } y \geq \lambda(t^2 + (\lambda x)^2)^{\frac{1}{2}} \\ 0 & \text{if } y \leq \lambda(t^2 + (\lambda x)^2)^{\frac{1}{2}} \end{cases}$$

The boundary of the level set which corresponds to $C = 0$ is given by the shape

$$X(t) = \left\{(x, y) : y = \lambda(t^2 + (\lambda x)^2)^{\frac{1}{2}}\right\}$$

the initial shape $t = 0$ corresponds to a corner given by the formula $y = \lambda^2|x|$. To fit this shape to the initial corner with angle α we must choose $\lambda = (\tan(\frac{\alpha}{2}))^{-\frac{1}{2}}$.

Finally, using a straightforward computation we deduce that the curvature measure at the scale t is given by the formula:

$$\text{curve}(u_\lambda)(t, x, y) = \begin{cases} \dfrac{\left(\frac{y}{\lambda}\right)^2 - (\lambda x)^2}{\left(\left(\frac{y}{\lambda^2}\right)^2 + (x\lambda^2)^2\right)^{\frac{3}{2}}} & \text{if } y \geq \lambda(t^2 + (\lambda x)^2)^{\frac{1}{2}} \\ 0 & \text{if } y \leq \lambda(t^2 + (\lambda x)^2)^{\frac{1}{2}} \end{cases}$$

At the scale t, the extremum of the above function is attained in the point $(0, \lambda t)$ which represents the location of the corner. □

We notice that the point $(0, \lambda t)$ is a local maximum of the curvature in any direction and not only along the normal direction of the gradient, which is the usual criterium in the computer vision community. From a numerical point of view, it means that we can look for local maxima of the curvature in any direction.

4.1. Multiscale Analysis of Multiple Junctions

To fix ideas we will consider a multiple junction as an image $u_0(x, y)$ given by a collection of corners which correspond to characteristic functions with different grey level values. So a multiple junction is determined by n grey levels $\{K_1 < K_2 < \cdots < K_{n-1} < K_n\}$ and n angles $\{\alpha_1, \alpha_2 \ldots, \alpha_n\}$ (see Fig. 3).

We recall that due to the Morphological invariance of AMSS the evolution of a Shape in the image only

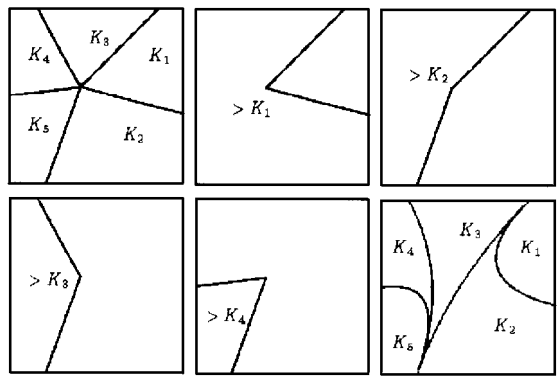

Figure 3. Multiple junction level set analysis. We represent, on the top-left, a multiple junction $u_0(x, y)$ with 5 different grey-levels $\{K_1 < K_2 < K_3 < K_4 < K_5\}$. From left to right and from top to bottom we represent 4 corners which correspond to the level sets $X_i = \partial\{(x, y)u_0(x, y) > K_i\}$ and, on the bottom-right, we represent the evolution of the multiple junction for a scale $t > 0$.

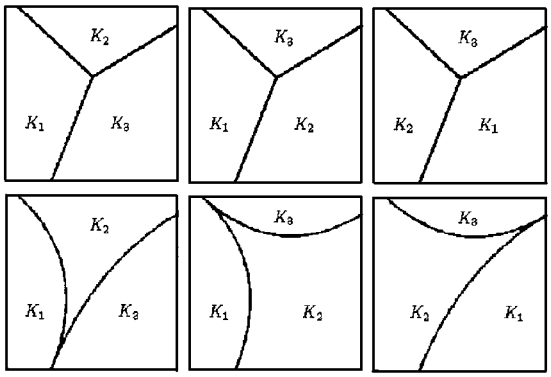

Figure 4. Trihedral vertex evolution. In the top we represent 3 different distributions of grey levels $K_1 < K_2 < K_3$ and at the bottom we represent the evolution which corresponds to each distribution of grey-levels for a scale $t > 0$.

depends on its geometry and not on other level sets present in the image. Using this argument we can separate the analysis of a multiple junction into the analysis of several corners. Indeed, if we take the Shape $X_i = \partial\{(x, y) : u_0(x, y) > K_i\}$, we have that, in the case $i = 1$, X_i corresponds to a single corner (see Fig. 3) and therefore it evolves as an isolated corner. If $i = 2$, X_i can be a single corner or the collection of X_1 and another corner. In the case of a single corner, X_2 evolves as an isolated corner. If X_2 is composed of X_1 and another corner, as we know that X_1 evolves as an isolated corner, we have that the another corner evolves also as an isolated corner. By using the same argument for any X_i, we can deduce that the multiple junction evolves as a collection of isolated corners. Of course, the way in which the corners evolve depends on the distribution of the grey-level $\{K_1 < K_2 < \cdots < K_{n-1} < K_n\}$ along the multiple junction. For instance, in Fig. 4 we present 3 different evolutions of a trihedral vertex following 3 different distributions of grey levels $K_1 < K_2 < K_3$.

Remark. If for some i, j we have that $K_i = K_j$ then we can loss the uniqueness in the evolution of the Shape in the sense that the same shape can evolve in different ways across the scales. Notice that this is not possible in the linear gaussian scale-space where the evolution of any shape is determined in a unique way. A classical example is a checkerboard surface (see (Fig. 5). Indeed, in this case the shape X_1 is a collection of two corners but we can not deduce, in a unique way, the evolution of the Shape because there are several

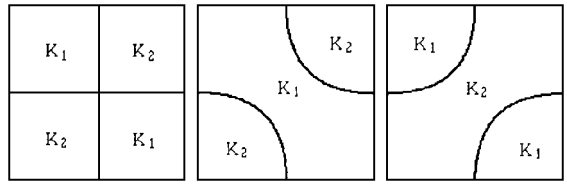

Figure 5. Checkerboard surface evolution. On the left we represent a checkerboard surface. In the middle and on the right we represent 2 possibilities in the evolution of the Shape.

possibilities in the choice of the configuration of the corners (see Fig. 5). We notice that the nonuniqueness of the solution is possible because of the discontinuities of the characteristic functions. In the case of smooth initial data the viscosity solution of the equation is unique.

5. Discretization of AMSS

First, we remove the scale dependence of the differential operator of the differential equation associated to the Multiscale Analysis AMSS. We notice that if we take $u(t, x, y) = v(\frac{3}{4}t^{\frac{4}{3}}, x, y)$ where $v(\cdot)$ is a solution of AMSS, then $u(\cdot)$ satisfies the differential equation

$$u_t = \left(u_y^2 u_{xx} - 2u_x u_y u_{xy} + u_x^2 u_{yy}\right)^{\frac{1}{3}} \tag{6}$$

then, by a simple rescaling we can remove the dependence in t of the differential operator of AMSS.

Instead of AMSS, we are going to discretize this equivalent equation by using finite differences. We shall introduce an explicit scheme which uses a fixed stencil of 3×3 points to discretize the differential operators. For simplicity, we assume that the spatial increment Δx is the same in the x-axis and the y-axis. We approach the first derivatives u_x and u_y in a point (i, j) of the lattice by using the following linear scheme:

$$(u_x)_{i,j} = \frac{2(u_{i+1,j} - u_{i-1,j}) + u_{i+1,j+1} - u_{i-1,j+1} + u_{i+1,j-1} - u_{i-1,j-1}}{8\Delta x} + \mathcal{O}(\Delta x^2)$$

$$(u_y)_{i,j} = \frac{2(u_{i,j+1}, -u_{i,j-1}) + u_{i+1,j+1} - u_{i+1,j-1} + u_{i-1,j+1} - u_{i-1,j-1}}{8\Delta x} + \mathcal{O}(\Delta x^2)$$

To discretize the operator

$$\Im(u) = u_y^2\, u_{xx} - 2u_x u_y\, u_{xy} + u_x^2\, u_{yy}$$

We write

$$u_{i+1,j} = u_{i,j} + \Delta x (u_x)_{i,j} + \frac{\Delta x^2}{2}(u_{xx})_{i,j} + \mathcal{O}(\Delta x^3),$$

we seek for some constants $\lambda_0, \lambda_1, \lambda_2, \lambda_3, \lambda_4$, such that

$$\begin{aligned}\Im(u)_{i,j} = \frac{1}{\Delta x^2}(&-4\lambda_0 u_{i,j} + \lambda_1(u_{i,j+1} + u_{i,j-1}) \\ &+ \lambda_2(u_{i+1,j} + u_{i-1,j}) \\ &+ \lambda_3(u_{i+1,j-1} + u_{i-1,j+1}) \\ &+ \lambda_4(u_{i+1,j+1} + u_{i-1,j-1})\big) + \mathcal{O}(\Delta x^2) \qquad (7)\end{aligned}$$

and the same relation for the other points of the stencil. By feeding (7) with these relations, we obtain four relations between our five coefficients

$$\begin{cases} \lambda_1 = 2\lambda_0 - u_y^2 \\ \lambda_2 = 2\lambda_0 - u_x^2 \\ \lambda_3 = -\lambda_0 + 0.5\big(u_y u_x + u_x^2 + u_y^2\big) \\ \lambda_4 = -\lambda_0 + 0.5\big(-u_y u_x + u_x^2 + u_y^2\big) \end{cases} \qquad (8)$$

There remains one degree of freedom for our coefficients given by the choice of λ_0. We shall choose λ_0 as a function of (u_x, u_y), (i.e., $\lambda_0 = \lambda_0(u_x, u_y)$), following some stability and geometric invariance criteria. Denoting by $u_{i,j}^n$ an approximation of $u(i\Delta x, j\Delta x, n\Delta t)$ we can write our explicit scheme as

$$u_{i,j}^{n+1} = u_{i,j}^n + \Delta t (\Im(u^n)_{i,j})^{\frac{1}{3}} \qquad (9)$$

As it was showed in (Alvarez and Morel, 1994) the stability of this scheme is closely related to the positivity of the coefficients $\lambda_1, \lambda_2, \lambda_3, \lambda_4$. Therefore, we must seek for λ_0 such that $\lambda_1, \lambda_2, \lambda_3, \lambda_4 \geq 0$. Unfortunately, because of the relations between the coefficients, it is impossible to obtain these relations, except for particular values of (u_x, u_y) given by the relation $|u_x| = |u_y|$. Indeed, we remark that in the region where $\{u_x \geq u_y \geq 0\}$,

$$\lambda_1 \geq \lambda_2 \quad \text{and} \quad \lambda_3 \geq \lambda_4$$

But

$$\lambda_2(u_x, u_y) \geq 0 \Rightarrow \lambda_0(u_x, u_y) \geq \frac{u_x^2}{2}$$

$$\lambda_4(u_x, u_y) \geq 0 \Rightarrow \lambda_0(u_x, u_y) \leq \frac{u_x^2 + u_y^2 - u_x u_y}{2}$$

So, we cannot find $\lambda_0(u_x, u_y)$ satisfying both inequalities, since

$$\frac{u_x^2}{2} \geq \frac{u_x^2 + u_y^2 - u_x u_y}{2}$$

In order to have the maximum of stability we choice, as function $\lambda_0(u_x, u_y)$, an average of the boundary functions:

$$\lambda_0(u_x, u_y) = \frac{2u_x^2 + u_y^2 - u_x u_y}{4} \qquad (10)$$

The coefficients $\lambda_0, \lambda_1, \lambda_2, \lambda_3, \lambda_4$ are given by the formula

$$\begin{cases} \lambda_0 = \begin{cases} 0.25\big(2u_x^2 + u_y^2 - |u_x u_y|\big) & \text{if } |u_x| \geq |u_y| \\ 0.25\big(2u_y^2 + u_x^2 - |u_x u_y|\big) & \text{if } |u_y| < |u_x| \end{cases} \\ \lambda_1 = 2\lambda_0 - u_y^2 \\ \lambda_2 = 2\lambda_0 - u_x^2 \\ \lambda_3 = -\lambda_0 + 0.5\big(u_x u_y + u_x^2 + u_y^2\big) \\ \lambda_4 = -\lambda_0 + 0.5\big(-u_x u_y + u_x^2 + u_y^2\big) \end{cases}$$

Remark. We would like to point out some arguments to justify the choice of this scheme to discretize AMSS instead of other schemes proposed in the literature. Sapiro and Tannenbaum (1993) propose a numerical scheme based on a Osher and Sethian (1988) idea. They implement the second order differential operator of the right part of Eq. (1) using central derivatives:

$$\begin{aligned} u_x &= \frac{u_{i+1,j}^n - u_{i-1,j}^n}{2\Delta x} \\ u_{xx} &= \frac{u_{i+1,j}^n + u_{i-1,j}^n - 2u_{i,j}^n}{\Delta x^2} \\ u_{xy} &= \frac{u_{i+1,j+1}^n + u_{i-1,j-1}^n - u_{i-1,j+1}^n - u_{i+1,j-1}^n}{4\Delta x^2} \end{aligned}$$

We recall that in our analysis the choice of λ_0 corresponds to a degree of freedom in the scheme. The Sapiro and Tannenbaum scheme corresponds to the choice $\lambda_0 = 0.5(u_x^2 + u_y^2)$ instead of (10). The main difference is that this choice of λ_0 is not well adapted to the lattice in the sense that the behaviour of the differential operator in the lattice is completely different in the axes directions and in the diagonals directions. In particular, we have not invariance of the scheme under rotations of angle $\frac{\pi}{4}$.

Cohignac et al. (1993) propose some schemes to discretize AMSS. They discuss and compare finite

difference schemes, curve evolution schemes and set evolution schemes. In the case of finite difference squemes, they propose, in particular, one scheme which is close to the scheme that we present in this paper. It corresponds to a choice of λ_0 given by:

$$\lambda_0 = 0.5\left(u_x^2 + u_y^2\right) - u_x^2 + \frac{u_x^4}{u_x^2 + u_y^2},$$

the main difference with respect to our choice of λ_0 is that they obtain that λ_0 is a smoother function with respect to the variation of the direction of the gradient but, on the other hand, this scheme needs supplementary divisions to be computed which can produce numerically instabilities when $u_x^2 + u_y^2$ is near to zero.

Next, we are going to present some numerical results using this algorithm to compute AMSS across the scales on different initial images. We assume (without any loss of generality) $\Delta x = 1$. We compute the solution of the Eq. (6), to recover the solution of AMSS we must do the rescaling using the formula

$$t = \left(\frac{4}{3} n \Delta t\right)^{\frac{3}{4}}$$

where n is the number of iterations and Δt the discretization step. In what follows we will take $\Delta t = 0.025$.

6. Application to Corner Analysis

To apply AMSS to corner analysis, the first problem to solve is how to identify the evolution of a corner across the scales from a numerical point of view. To solve this problem we use the following criterion: a corner is represented by a local extremum of the differential operator $\frac{u_y^2 u_{xx} - 2u_x u_y u_{xy} + u_x^2 u_{yy}}{(u_x^2+u_y^2)^{\frac{3}{2}}}$. In the practical cases, when we deal with real pictures, we remove the denominator in the above expression in order to improve the robustness of the operator. We notice that the set local of extrema include the corners and other points that, in general do not represent corners, but the idea is that we can identify the corners following their evolution across the scales.

We take initially all the local extrema of the initial image. To do is, we compute numerically the above differential operator in the lattice and we define a local extremum as a point where the value of the differential operator is bigger (or lower) than the values of its 8 neighbors (we take a 3×3 stencil). We compute AMSS and we say that the local extremum has changed its position at the scale t if, at this scale, there exists a neighbor of the point whose value of the differential operator is bigger (or lower) than the value of the point itself. By iterating this procedure we obtain, for each local extremum (x_0, y_0) a chain of points (t_n, x_n, y_n) where (x_n, y_x) represents the position of the extremum at the scale t_n. Associated to this chain we can define the chain of distance to the initial point given by (t_n, d_n) where d_n is defined by $\sqrt{(x_n - x_0)^2 + (y_n - y_0)^2}$. As we have showed in Section 4, in the continuous case, the evolution of a corner is given by a straight line, therefore (t_n, d_n) must be a straight line and the slope of this straight line must identify the angle of the corner. Of course, in the numerical case, we cannot expect to match exactly these results because the representations of corners in a lattice and the numerical evolution of AMSS produce numerical errors. However, as we are going to see, the numerical results approach well the continuous analysis.

To fit the chain (t_n, d_n) to a straight line, we compute, by standard techniques two constant (a, b) by

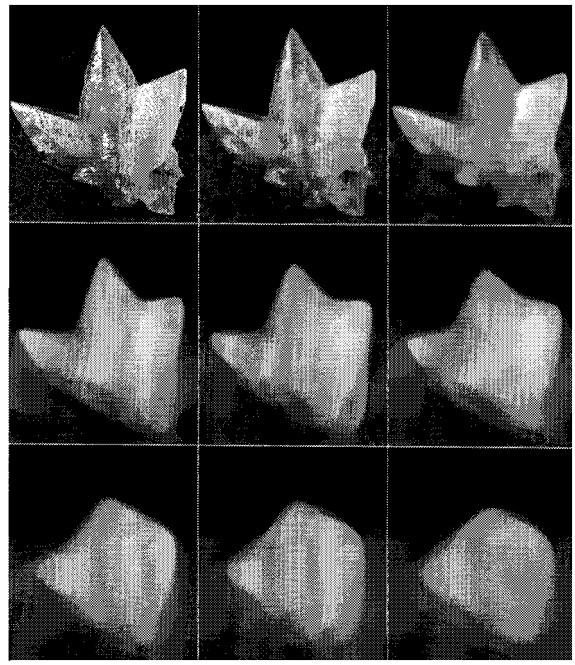

Figure 6. In this picture we present the evolution across the scales using AMSS of a real image (190×220 pixels) which represents the picture of a calcite stone. From left to right and from top to down we represent the analysis for the scales: $t = 0., 2.13, 4.26, 9.96, 12.80, 16.37, 19.92, 22.76, 25.62$.

minimizing, with respect to a, b the functional:

$$\sum_n (at_n + b - d_n)^2$$

where a represents the slope of the straight line. We use, as approximation error, the number:

$$Error = \frac{\sum_n (at_n + b - d_n)^2}{N^2} \tag{11}$$

where N represents the number of points of the chain.

We recall that the point (x_n, y_n) moves along the bisector line of the corner and that the slope a characterizes the angle α of the corner $a = (\tan(\frac{\alpha}{2}))^{-\frac{1}{2}}$. With this information we can recover the location and orientation of the corner in the image.

Here, we present one technique to follow the evolution of the corners using AMSS and to compute an approximation error. But, of course, other choices are possible, including, for instance, other criteria to compute the chains (t_n, x_n, y_n), or to compute the approximation error. We notice that with this scheme you can extract only one chain for each extremum point (x_0, y_0). It means, in the particular case of multiple junctions we can lose information about the number of corners present in the multiple junction. We point out that we have focused our attention on the AMSS scale space from a conceptual point of view, and not in a computational accurate scheme to follow corners across the scales. However, as we will show, the experimental results are very promising.

Next, in Figs. 7, 8 and 9 we present some experimental results by using synthetic pictures which represent corners of angle $\frac{3\pi}{4}$, $\frac{\pi}{2}$, and $\frac{\pi}{4}$. A very important fact is that, as we are going to show, the approximation

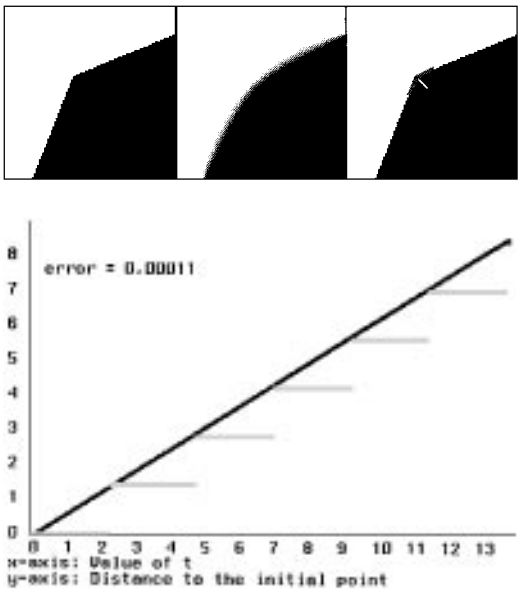

Figure 7. We present the evolution across the scales using AMSS of a corner of angle $\frac{3\pi}{4}$. The corner is included in a (100×100 pixels) image. We follow the evolution of the corner until the scale $t = 14$. On the left we present the initial image, in the middle we present the image at the scale $t = 14$, and on the right we present the evolution and location of the corner according to the information of the bisector line and the displacement velocity a. In the graph below, we represent (with grey-levels) the chain (t_n, d_n) where the jumps represent the scale where the extremum changes its position. Finally, with black color, we represent the approximation straight line, where $a \simeq 0.61$ and $b \simeq -0.05$. The theoretical expected values, using the continuous analysis are $a \simeq 0.6436$ and $b = 0$. The approximation error is $Error \simeq 0.00011$.

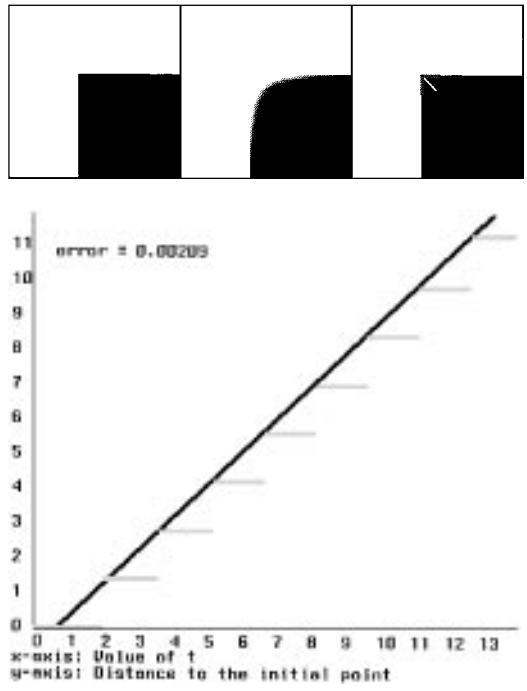

Figure 8. We present the evolution across the scales using AMSS of a corner of angle $\frac{\pi}{2}$. The corner is included in a (100×100 pixels) image. We follow the evolution of the corner until the scale $t = 14$. On the left we present the initial image, in the middle we present the image at the scale $t = 14$, and on the right we present the evolution and location of the corner according to the information of the bisector line and the displacement velocity a. In the graph below, we represent (with grey-levels) the chain (t_n, d_n) where the jumps represent the scale where the extremum changes its position. Finally, with black color, we represent the approximation straight line, where $a \simeq 0.93$ and $b \simeq -0.51$. The theoretical expected values, using the continuous analysis are $a = 1$ and $b = 0$. The approximation error is $Error \simeq 0.00209$.

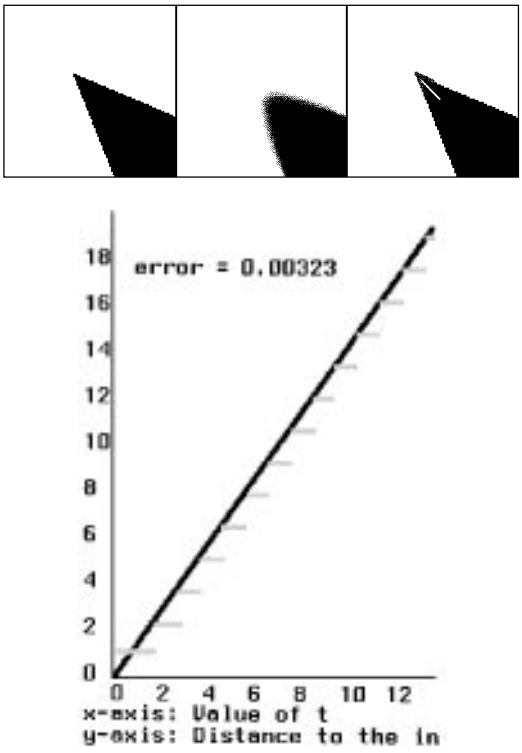

Figure 9. We present the evolution across the scales using AMSS of a corner of angle $\frac{\pi}{4}$. The corner is included in a (100×100 pixels) image. We follow the evolution of the corner until the scale $t = 14$. On the left we present the initial image, in the middle we present the image at the scale $t = 14$, and on the right we present the evolution and location of the corner according to the information of the bisector line and the displacement velocity a. In the graph below, we represent (with grey-levels) the chain (t_n, d_n) where the jumps represent the scale where the extremum changes its position. Finally, with black color, we represent the approximation straight line, where $a \simeq 1.4$ and $b \simeq -0.01$. The theoretical expected values, using the continuous analysis are $a \simeq 1.55$ and $b = 0$. The approximation error is $Error \simeq 0.00303$.

error (11) is very little in all cases. It means that the chain (t_n, d_n) fits very well a straight line.

In Fig. 10, we present some experimental results about the evolution across the scales of singularities as multiple junctions, trihedral vertexes and checkerboard type surfaces. We notice that from a numerical point of view, there is only 1 possibility in the evolution of a Shape across the scales. So the nonuniqueness in the continuous case does not produce nonuniqueness in the numerical scheme but it produces instabilities in the scheme in the sense that changing the value of a few number of pixels near the singularities you can produce completely different evolutions.

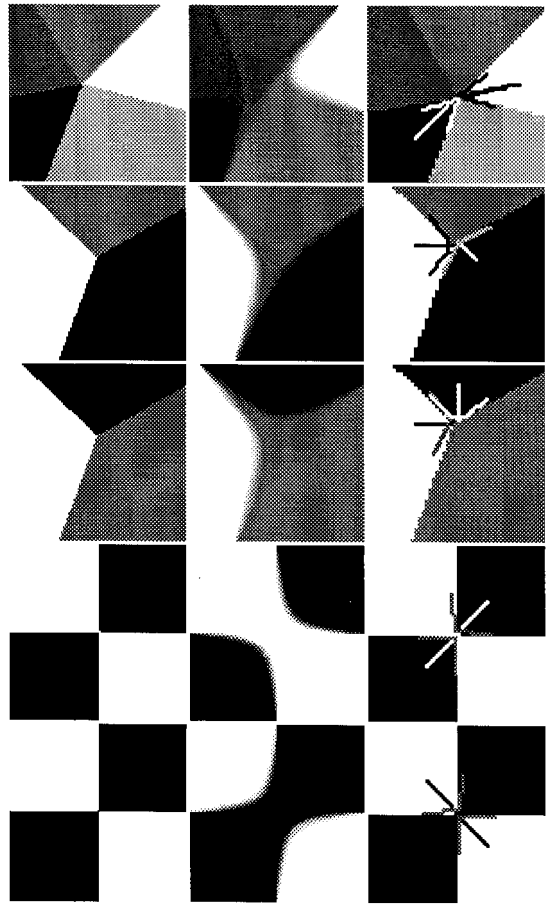

Figure 10. From top to bottom we present the evolution across the scales using AMSS of 1 multiple junction, 2 trihedral vertexes with different distributions of grey-levels and 2 checkerboard type surfaces where we have changed the value of the grey-level of two central pixels to point out the nonuniqueness in the evolution of the Shape. For each image, on the left we present the original image, in the middle we present the image at the scale $t = 14$, and on the right we present a zoom of the singularity with the evolution and location of the corners extracted following our analysis. The computed values of a and the approximation error $Error$ for each corner are the following: **Image 1:** (up) black chain: $a \simeq 1.25$, $Error \simeq 0.00572$, white chain $a \simeq 1.26$, $Error \simeq 0.00238$, **Image 2:** black chain: $a \simeq 0.77$, $Error \simeq 0.0015$, white chain $a \simeq 0.59$, $Error \simeq 0.0001$, **Image 3:** black chain: $a \simeq 0.75$, $Error \simeq 0.00134$, white chain $a \simeq 0.78$, $Error \simeq 0.00438$, **Image 4:** right chain: $a \simeq 0.86$, $Error \simeq 0.00498$, left chain $a \simeq 0.93$, $Error \simeq 0.00274$, **Image 5:** left chain: $a \simeq 0.86$, $Error \simeq 0.00498$, right chain $a \simeq 0.94$, $Error \simeq 0.00281$.

In Fig. 11, we present the application of our analysis to a real image which represents a calcite stone. We analyze the evolution of 565 local extrema of the image until the scale $t = 14$, we put in order all the associated chains (t_n, d_n) according to the value of the

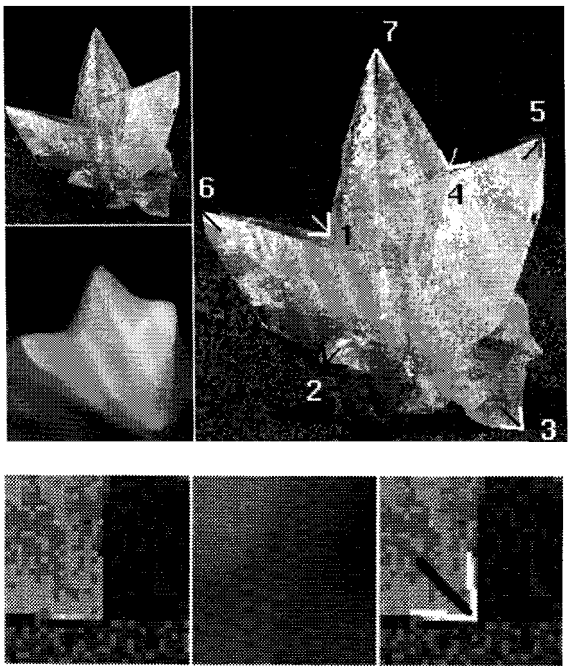

Figure 11. We present the evolution across the scales (until the scale $t = 14$) of the 7 chains where the approximation errors are lowest for the calcite stone image. On the left we present the initial image, in the one below we present the image at the scale $t = 14$, and on the right we present the evolution of the seven chains (t_n, d_n) and the corners detected by the analysis. The values of the approximation error and a for each chain are: **chain 1:** *Error* $\simeq 0.00044$, $a \simeq 0.95$, **chain 2:** *Error* $\simeq 0.00244$, $a \simeq 0.080$, **chain 3:** *Error* $\simeq 0.00379$, $a \simeq 1.0$, **chain 4:** *Error* $\simeq 0.00769$, $a \simeq 0.8$, **chain 5:** *Error* $\simeq 0.00771$, $a \simeq 1.03$, **chain 6:** *Error* $\simeq 0.008$, $a \simeq 1.2$, **chain 7:** *Error* $\simeq 0.01028$, $a \simeq 1.17$. In the figure below we present a zoom of the calcite image where a T-junction is detected.

approximation error (11). (Of course, we remove the trivial cases of chains which have only one or two points.) In Fig. 10 we present the 7 first chains in which the approximation error is lower. As we show, these chains correspond to the evolution of the most relevant corners present in the image. In figure below we present a zoom of the calcite image where a T-junction is detected.

7. Conclusions

In this paper we have analyzed the evolution across the scales of the corners present in an image, using the AMSS scale space. First, in the continuous case, we introduce a new family of travelling waves solutions of AMSS which characterize the evolution of initial shapes given by conics. Using the same kind of idea, we characterize the evolution of corners and we show that a corner evolves following a straight line across the scales and the slope of this straight line characterizes the angle of the corner. Due to the invariance properties of AMSS, this analysis in independent of the location and relative contrast of the corner with other shapes. From the numerical point of view, we present an algorithm to compute AMSS across the scales, and a procedure to follow the evolution of corners across the scales. By using this information we can extract the position of the most relevant corners of the image. To do it, we compute how well the evolution of an extremum of the curvature fits a straight line. We put in order all the extrema using as criterium the approximation error (to the straight line) and we show that the points which minimize this approximation error correspond to relevant corners. This error increases when the angle of the corner decreases. It is quite natural because the representation in a lattice of a corner and its evolution across the scales introduces more numerical perturbations when the angle of the corner is lower.

The AMSS scale space represents an alternative way to interpret and analyze image. AMSS focus the attention on the analysis of shapes following their geometry. This analysis is independent of other shapes present in the image, in other words, shapes evolve across the scales as isolated features and this property help us to analyze and identify them. The classical gaussian linear scale space tends to blend the information about the different shapes present in the image and the evolution of a shape depends on the relative contrast and location of other shapes present in the image. This fact can make difficult the analysis and identification of the shapes. The trihedral vertex analysis is a typical example of this situation. In the case of AMSS, a trihedral vertex is a simple collection of two corners and the evolution of the trihedral vertex is the evolution of two corners in an independent way. In the case of linear gaussian scale space, as it was notice by Deriche and Giraudon (1993) the analysis of a trihedral vertex is much more complex than the analysis of corners and it depends strongly on the contrast among the different surfaces.

References

Alvarez, L., Guichard, F., Lions, P.L., and Morel, J.M. 1992. Axiomatisation et nouveaux opérateurs de la morphologie mathematique. *C.R. Acad. Sci. Paris*, t.315, Série I, pp. 265–268.

Alvarez, L., Lions, P.L., and Morel, J.M. 1992. Image selective smoothing and edge detection by nonlinear diffusion (II). *SIAM Journal on Numerical Analysis*, 29:845–866.

Alvarez, L., Guichard, F., Lions, P.L., and Morel, J.M. 1993. Axioms and fundamental equations of image processing. *Arch. for Rat. Mech.*, t.123. 3:199–257.

Alvarez, L. and Mazorra, L. 1994. Signal and image restoration using shock filters and anisotropic diffusion. *SIAM Journal on Numerical Analysis*, 31(2):590–605.

Alvarez, L. and Morel, J.M. 1994. Formalization and computational aspects of image analysis. *Acta Numerica*, pp. 1–59.

Asada, H. and Brady, M. 1986. The curvature primal sketch. *IEEE Transactions on Pattern Analysis and Machine Intelligence*, 8(1).

Beaudet, P.R. 1978. Rotational invariant image operators. *4th Intern. Conf. Patt. Recog.*, Tokio, pp. 579–583.

Caselles, V. and Sbert, C. 1996. What is the best causal scale space for 3-D images?. In *SIAM Journal on Applied Math*, 56:1199–1246.

Catté, F., Dibos, F., and Koepfler, G. 1993. A morphological approach of mean curvature motion. Report 9310, CEREMADE. Université Paris Dauphine.

Cohignac, T., Eve, F., Guichard, F., Lopez, C., and Morel, J.M. 1993. Numerical analysis of the fundamental equation of image processing (to appear).

Crandall, M.G., Ishii, H., and Lions, P.L. 1992. User's guide to viscosity solution of second order partial differential equation. *Bull. AMS*, 27/1:1–67.

Deriche, R. and Giraudon, G. 1993. A computational approach for corner and vertex detection. *International Journal of Computer Vision*, 10(2):101–124.

Deriche, R. and Blaszka, T. 1993. Recovering and characterizing image features using an efficient model based approach. *Proc. IEEE Conference on Computer Vision and Pattern Recognition*, New York, pp. 14–17.

Deriche, R. 1994. Private communication.

Dreschler, L. and Nagel, H.H. 1982. On the selection of critical points and local curvature extrema of region boundaries for interframe matching. *Intern. Conf. Patt. Recog.*, pp. 542–544.

Faugeras, O. 1993. On the evolution of simple curves of the real projective plane. *C.R. Acad. Sci. Paris*, T.317, Série I (6):565–570.

Gage, M. and Hamilton, R.S. 1986. The heat equation shrinking convex plane curves. *J. Differential Geometry*, 23:69–96.

Grayson, M. 1987. The heat equation shrinks embedded plane curves to round points. *J. Differential Geometry*, 26:285–314.

Hummel, R. 1986. Representations based on zero-crossing in scale-space. *Proc. IEEE Computer Vision and Pattern Recognition Conference*, pp. 204–209.

Julesz, B. 1981. Textons, the elements of texture perception, and their interactions. *Nature*, Vol. 290.

Kitchen, L. and Rosenfeld, A. 1982. Gray-level corner detection. *Patt. Recog. Letter*, (1):95–102.

Koenderink, J.J. 1984. The structure of images. *Biol. Cybern.*, 50:363–370.

Lindeberg, T. 1993. Detecting salient blob-like image structures and their scales with a scale-space primal sketch: A method for focus-of-attention. *Intl. J. of Computer Vision*, 11(3):283–318.

Lopez, C. and Morel, J.M. 1992. Axiomatisation of shape analysis and application to texture hyperdiscrimination. *Proc. of the Trento Conference on Surface Tension and Movement by Mean Curvature*, De Gruyter Publishers: Berlin.

Mackworth, A. and Mokhtarian, F. 1986. Scale-based description and recognition of planar curves and two-dimensional shapes. *IEEE Transactions on Pattern Analysis and Machine Intelligence*, 8(1).

Mackworth, A. and Mokhtarian, F. 1992. A theory of multiscale, curvature-based shape representation for planar curves. *IEEE Trans. Pattern Anal. Machine Intell.*, 14:789–805.

Maragos, P. 1987. Tutorial on advances in morphological image processing and analysis. *Optical Engineering*, 26(7).

Marr, D. 1982. *Vision*. Freeman and Co.

Matheron, G. 1975. *Random Sets and Integral Geometry*. John Wiley: N.Y.

Merriman, B., Bence, J., and Osher, S. 1992. Diffusion generated motion by mean curvature. CAM Report 92-18, Dept. of Mathematics, University of California, Los Angeles CA 90024. 1555.

Merriman, B., Bence, J., and Osher, S. 1994. Motion of multiple junctions: A level set approach. *Journal of Computational Physics*, 112:334–363.

Morel, J.M. and Solimini, S. 1994. *Variational Methods in Image Segmentation*. Birkhauser.

Osher, S. and Sethian, J. 1988. Fronts propagating with curvature dependent speed: Algorithms based on the Hamilton-Jacobi formulation. *J. Comp. Physics*, 79:12–49.

Perona, P. and Malik, J. 1987. A scale space and edge detection using anisotropic diffusion. *Proc. IEEE Computer Soc. Workshop on Computer Vision*.

Rohr, K. 1994. Localization properties of direct corner detectors. *Journal of Mathematical Imaging and Vision*, 4:139–150.

Sapiro, G. and Tannenbaum, A. 1993. Affine invariant scale-space. *International Journal of Computer Vision*, 11(1):25–44.

Sapiro, G. and Tannenbaum, A. 1993. On invariant curve evolution and image analysis. *Indiana University Mathematics Journal*, 42(3):985–1009.

Sapiro, G. and Tannenbaum, A. 1994. On affine plane curve evolution. *Journal of Functional Analysis*, 119(1):79–120.

Serra, J. 1982. *Image Analysis and Mathematical Morphology*, Academic Press, Vol. 1.

Witkin, A.P. 1983. Scale-space filtering. *Proc. of IJCAI*, Karlsruhe, pp. 1019–1021.

Yuille, A. and Poggio, T. 1986. Scaling theorems for zero crossings. *IEEE Transactions on Pattern Analysis and Machine Intelligence*, Vol. 8.